Sign of line tension in liquid bridge stability

Riccardo Rosso and Epifanio G. Virga
Dipartimento di Matematica, Istituto Nazionale di Fisica della Materia, Università di Pavia, Via Ferrata 1, 27100 Pavia, Italy
(Received 15 March 2004; published 14 September 2004)

We apply the stability criterion we recently proposed for a general wetting functional [Phys. Rev. E **68**, 012601 (2003)] to find out whether straight liquid bridges can be stable when subject to line tension of either sign. Our main conclusion is that, even when the line tension is negative, a straight liquid bridge can be stable, and so observable, provided that the line tension is not too large in absolute value.

DOI: 10.1103/PhysRevE.70.031603 PACS number(s): 68.08.Bc

I. INTRODUCTION

The concept of line tension was introduced by Gibbs [1] to describe the excess free energy arising along a three-phase line, that is, along a curve where three distinct phases coexist. In Gibbs's original formulation, the line tension was introduced as the analog to the surface tension for a two-phase surface. Line tension is relevant to equilibrium only at nanometric length scales, which have recently become accessible to experiments [2–5]. However, extracting information on line tension from these experiments is a difficult task, and so different results are available that attribute to the line tension values also differing by many orders of magnitude (typically, these values range from 10^{-12} to 10^{-5} N). Moreover, even the sign of the line tension is subject to controversy. Similar ambiguities also arise in theoretical models that indeed predict disparate values for the line tension and disagree on its sign as well. It has been claimed that line tension cannot be negative, by a stability argument [6–8]. Recently, we proposed a general stability criterion for wetting functionals that could help to explore the consequences of negative line tensions [9,10]. In fact, in Ref. [9] we already performed a stability analysis for a liquid bridge lying on a flat substrate, in the special case where the contact angle is $\pi/2$. We proved that, although a negative line tension favors the onset of instability, if its modulus is not too large, the instability occurs only for modes that are too wiggly to be admissible within the range of validity of the model. It is our purpose here to extend such a stability analysis to see the influence of the contact angle when it ranges in the whole interval $(0,\pi)$.

Liquid bridges are special droplets, which we expect to be unstable when they become too slender, as suggested by the classical Rayleigh instability that should indeed be reproduced exactly in this context when the contact angle is $\pi/2$ and the line tension is absent. The major conclusion of our study is that liquid bridges with negative line tension can also be stable, and so observable, provided that the line tension is not too large in absolute value. Nonetheless, as our analysis will show, this conclusion, which here is rigorously proved for liquid bridges, cannot be naively extended to other droplet morphologies, although one would expect it to be qualitatively valid in general.

The paper is organized as follows. In Sec. II, we describe the mathematical model employed here and we recall our stability criterion for the reader's ease. In Sec. III we solve the eigenvalue problem involved in our criterion by combining both graphical and numerical methods. Finally, Sec. IV collects our conclusions. Most of the mathematical details left out in the main body of the paper are explained in the closing Appendix.

II. MATHEMATICAL SETTING

The line tension along a three-phase contact can be defined in rather different ways. Here, we use a continuum approach where the excess free energy is modeled as a line integral on the *contact line* $\mathcal{C}$, that is, the contour where the liquid droplet, the substrate, and the environment fluid are in contact. Moreover, for simplicity, we assume that the line tension γ is constant along $\mathcal{C}$. Thus, the free-energy functional $\mathcal{F}$ that governs the equilibrium of a liquid droplet $\mathcal{B}$ is given by

$$\mathcal{F}[\mathcal{B}] = \tau \int_{S} da + (\tau - w) \int_{S_*} da + \gamma \int_{C} ds, \qquad (1)$$

where $\tau > 0$ is the surface tension between the droplet and the environment fluid, $\mathcal{S}$ is the surface of the droplet in contact with the environment, and $\mathcal{S}_*$ is the surface of the droplet in contact with the substrate. The positive constant w, referred to as the *adhesion potential*, accounts for the interaction between the droplet and the substrate, which is assumed flat and chemically homogeneous. Finally, a is the area measure on $\partial\mathcal{B} = \mathcal{S} \cup \mathcal{S}_*$ and s is the arclength along $\mathcal{C}$. To arrive at the Euler-Lagrange equation associated with the functional $\mathcal{F}$, we perturb a point $p \in \partial\mathcal{B}$ into $p_\varepsilon = p + \varepsilon \mathbf{u} + \varepsilon^2 \mathbf{v}$, where $\mathbf{u}$ and $\mathbf{v}$ are regular vector fields defined on $\partial\mathcal{B}$. As explained in Ref. [9], the second-order term $\mathbf{v}$ in the perturbation is indeed needed to preserve up to second order the constraints that a droplet on a substrate is subject to. The Euler-Lagrange equation of the functional (1) is obtained by setting the first variation $\delta\mathcal{F}$ of $\mathcal{F}$ equal to zero:

$$\delta\mathcal{F}[\mathbf{u}] := \left. \frac{d\mathcal{F}}{d\epsilon} \right|_{\epsilon=0} = 0.$$

In the absence of gravity or other external fields, the Euler-Lagrange equation requires $\mathcal{S}$ to be a surface with constant mean curvature, which, in particular, makes a circular cylinder an admissible solution. In general, along the contact line $\mathcal{C}$, the following natural boundary condition is to be satisfied:

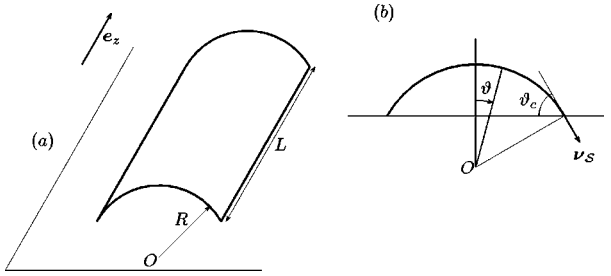

FIG. 1. (a) Sketch of a liquid bridge lying on a flat, homogeneous substrate. The bridge is a straight circular cylindrical sector, of length L in the $\mathbf{e}_z$ direction. (b) Every planar cross section of the bridge orthogonal to $\mathbf{e}_z$ is a circular sector of radius R, centered at the point O. The contact angle ϑ_c is the angle between the substrate and the bridge's tangent plane along the contact line $\mathcal{C}$. The unit vector $\boldsymbol{\nu}_S$ is the conormal of $\mathcal{C}$ on $\mathcal{S}$, that is, the outward unit vector orthogonal to $\mathcal{C}$ on $\mathcal{S}$. Finally, ϑ is the polar angle, which is often employed below.

$$\tau \cos \vartheta_c + \tau - w = \gamma \kappa_g^*, \tag{2}$$

where ϑ_c is the *contact angle*, which here is the angle between the substrate and the bridge's tangent plane along the contact line $\mathcal{C}$ (see Fig. 1), and κ_g^* is the geodesic curvature of $\mathcal{C}$ relative to the substrate [9,11]. Since both τ and w are taken to be constant, Eq. (2), which is the celebrated Young equation, requires that ϑ_c is constant along the contact line $\mathcal{C}$.

The stability of any equilibrium configuration for a drop is related to the sign of the second variation of $\mathcal{F}$, defined as

$$\delta^2 \mathcal{F}[\mathbf{u}] := \left. \frac{d^2 \mathcal{F}}{d\epsilon^2} \right|_{\epsilon=0}.$$

Precisely, the notion of stability employed throughout this paper is the one that would more properly be named *local*: according to its definition, an equilibrium shape $\mathcal{S}$ is said to be stable whenever the second variation $\delta^2 \mathcal{F}$ is positive for all admissible perturbations of $\mathcal{S}$ (see, e.g., Ref. [12], Chap. V).

The only droplets we shall consider here are incompressible liquid *bridges*, that is, bodies resembling cylindric lenses with axis along a given direction, say $\mathbf{e}_z$ (see Fig. 1). The cross section of a bridge with every plane orthogonal to $\mathbf{e}_z$ is a circular sector of radius R; the contact line $\mathcal{C}$ is split into two congruent straight-line segments of length L. Clearly, in this case $\kappa_g^*=0$, and by applying the general results obtained in Ref. [9] we can write the second variation of the free-energy functional (1) as

$$\delta^2 \mathcal{F}[\mathbf{u}] = \tau \int_S \left\{ |\nabla_s u_\nu|^2 - \frac{1}{R^2} u_\nu^2 \right\} da + \int_{\mathcal{C}} \left\{ \gamma (u_s')^2 - \frac{\tau}{R} \cos \vartheta_c \sin \vartheta_c u_s^2 \right\} ds, \tag{3}$$

where u_ν is the component of the perturbation $\mathbf{u}$ along the unit normal $\boldsymbol{\nu}$ to $\mathcal{S}$, and u_s is related to u_ν on $\mathcal{C}$ through the equation

$$u_\nu = \sin \vartheta_c u_s. \tag{4}$$

No explicit contribution in the second variation (3) arises from the adhesion potential w: this follows from the constraint $u_\nu=0$ imposed on the perturbation $\mathbf{u}$ on $\mathcal{S}_*$ to guarantee that $\mathbf{u}$ maps $\mathcal{S}_*$ onto another surface on the substrate (see Refs. [9,10] for further details).

According to Eq. (4), we can replace u_s with u_ν in Eq. (3) to make the second variation $\delta^2 \mathcal{F}$ a quadratic functional of u_ν. $\delta^2 \mathcal{F}$ is positive whenever its minimum on the unit sphere in $L^2(\mathcal{S})$ is positive. Thus, we subject $\delta^2 \mathcal{F}$ to the normalization constraint

$$\int_S u_\nu^2 da = 1, \tag{5}$$

which, since the liquid bridge is taken to be incompressible, supplements the constraint on the average of u_ν,

$$\int_S u_\nu da = 0. \tag{6}$$

As discussed in Ref. [9], the minimum of the functional (3) on the manifold (5) coincides with the minimum eigenvalue μ of the following problem:

$$\Delta_s u_\nu + \left(\mu + \frac{1}{R^2} \right) u_\nu + \lambda = 0 \ \text{ on } \ \mathcal{S}, \tag{7}$$

$$\sin^2 \vartheta_c \nabla_s u_\nu \cdot \nu_S - \xi u_\nu'' - \frac{1}{R} \sin \vartheta_c \cos \vartheta_c u_\nu = 0 \ \text{ along } \ \mathcal{C}. \tag{8}$$

Here, ∇_s and Δ_s are, respectively, the surface gradient and the surface Laplacian defined on $\mathcal{S}$, a prime denotes differentiation along the arclength s of $\mathcal{C}$, and λ is the Lagrange multiplier associated with the constraint (6). Moreover, the unit vector $\boldsymbol{\nu}_S$ is the unit conormal of $\mathcal{C}$ on $\mathcal{S}$, that is, the outward unit vector orthogonal to $\mathcal{C}$ on $\mathcal{S}$ (see Fig. 1). Finally, the ratio

$$\xi := \frac{\gamma}{\tau}, \tag{9}$$

which bears the physical dimensions of a length, is a central quantity in our development; in principle, like γ, it can have either sign. The free surface $\mathcal{S}$ of the bridge can easily be described in the cylindrical coordinates ϑ and z shown in Fig. 1: formally,

$$\mathcal{S} := \{(\vartheta, z) | \vartheta \in [-\vartheta_c, \vartheta_c], z \in [0, L]\}.$$

Here we set $u(\vartheta, z) := u_\nu(\vartheta, z)$, for simplicity. Since

$$\nabla_s u \cdot \boldsymbol{\nu}_S = \frac{\partial u}{\partial \vartheta} \ \text{ and } \ \Delta_s u = \frac{1}{R^2} \frac{\partial^2 u}{\partial \vartheta^2} + \frac{\partial^2 u}{\partial z^2},$$

we can recast Eqs. (7) and (8) as

$$\frac{1}{R^2} \frac{\partial^2 u}{\partial \vartheta^2} + \frac{\partial^2 u}{\partial z^2} + \left(\mu + \frac{1}{R^2} \right) u + \lambda = 0, \tag{10}$$

$$\frac{1}{R}\sin^2\vartheta_c\frac{\partial u}{\partial\vartheta}\bigg|_{\vartheta=\vartheta_c} - \xi\frac{\partial^2 u}{\partial z^2}\bigg|_{\vartheta=\vartheta_c} - \frac{1}{R}\sin\vartheta_c\cos\vartheta_c u(\vartheta_c,z) = 0. \tag{11}$$

We think of the bridge as being infinite along its axis: in the same spirit as the classical Rayleigh instability, we treat L as the length over which typical distortions of the bridge's shape take place, and so we require that

$$u(\vartheta,0) = u(\vartheta,L) = 0, \ \forall\ \vartheta\in[0,\vartheta_c]. \tag{12}$$

For simplicity, we also limit our attention to symmetric perturbations, which satisfy the condition

$$\frac{\partial u}{\partial\vartheta}\bigg|_{\vartheta=0} = 0, \ \forall\ z\in[0,L]. \tag{13}$$

The cross section's size R is taken throughout as given, although it will enter our discussion only through two dimensionless ratios, namely, R/L and R/ξ. For most materials $|\xi|$ is much smaller than any macroscopic length, and one would be led to assume that $R/|\xi|\gg 1$. Here this assumption is not made, as we also wish to consider the possibility that R is not a macroscopic length. Rayleigh's instability, which in a full liquid cylinder happens when $L\geqslant 2\pi R$, will be taken as a reference case below: in the absence of line tension, it should be reproduced by a liquid bridge when $\vartheta_c=\pi/2$.

III. STABILITY ANALYSIS

This section, which is divided into two parts, concerns the stability analysis of liquid bridges against perturbations satisfying both the incompressibility constraint (6) and Eqs. (12) and (13). In the first part, we suppose $\xi>0$ and prove general results that are then specialized to the asymptotic limits where either the line tension is very small or it is very large. In the second part, we study the case where $\xi<0$.

A. Positive line tension

Following the approach adopted by Roy and Schwartz [13], we look for solutions to Eqs. (10) and (11) in the form

$$u(\vartheta,z) = u_0(\vartheta) + \sum_{n=1}^{\infty}\sin\left(\frac{n\pi}{L}z\right)u_n(\vartheta), \tag{14}$$

with $n\in\mathbb{N}$. Since for a cylinder the incompressibility condition (6) reads

$$\int_0^L dz\int_0^{\vartheta_c} u(\vartheta,z)d\vartheta = 0,$$

we conclude from Eq. (14) that only even modes occur, that is,

$$u(\vartheta,z) = u_0(\vartheta) + \sum_{n=1}^{\infty}\sin\left(\frac{2n\pi}{L}z\right)u_n(\vartheta). \tag{15}$$

Moreover, the constraint (6) reduces to a restriction on the lowest mode $u_0(\vartheta)$,

$$\int_0^{\vartheta_c} u_0(\vartheta)d\vartheta = 0. \tag{16}$$

However, imposing Eq. (12) amounts to setting $u_0(\vartheta)\equiv 0$ and so the projection of Eq. (10) onto the eigenspace corresponding to $n=0$ yields $\lambda=0$ immediately. For higher modes, inserting Eq. (15) into Eq. (10) yields

$$\ddot{u}_n + (\mu R^2 + 1 - \varrho_n)u_n = 0, \ \forall\ n\geqslant 1, \tag{17}$$

where we have set

$$\varrho_n := \left(\frac{2\pi nR}{L}\right)^2, \tag{18}$$

and an overdot stands for differentiation with respect to ϑ. Finally, by replacing Eq. (15) in Eq. (11) we readily obtain

$$\sin^2\vartheta_c\dot{u}_n(\vartheta_c) + \left(\frac{\xi}{R}\varrho_n - \sin\vartheta_c\cos\vartheta_c\right)u_n(\vartheta_c) = 0, \ \forall\ n\geqslant 1, \tag{19}$$

where every function u_n obeys

$$\dot{u}_n(0) = 0, \tag{20}$$

as a consequence of Eq. (13).

Our purpose here is to find all the modes for which Eqs. (17)–(20) possess a nontrivial solution with $\mu>0$. If these are not all possible modes, then the bridge will be found unstable against the ones for which $\mu<0$. Since the ratio R/L is not fixed, we will label every mode by ϱ_n: our strategy will be to find for each admissible ϱ_n the corresponding eigenvalue μ. Guided by the classical Rayleigh instability, one would expect that for ϱ_n sufficiently large, a bridge can always be made stable: our analysis will show the effect of line tension, and especially of its sign, on this expectation.

The solutions to Eqs. (17)–(20) have different qualitative behaviors, according to the sign of the parameter

$$\sigma_n := \mu R^2 + 1 - \varrho_n. \tag{21}$$

When $\sigma_n=0$, the only nontrivial solution of Eq. (17) that also satisfies Eq. (20) is $u_n(\vartheta)=B$, with B a constant. The corresponding mode depends only upon z: hereafter, we shall refer to it as to a *linear* mode. The constant B can be determined uniquely by imposing the constraint (5). Equation (19) gives the necessary conditions for this mode to exist, that is,

$$0 < \varrho_n = 1 + \mu R^2 = \frac{R}{\xi}\sin\vartheta_c\cos\vartheta_c. \tag{22}$$

It follows from these equations that, if $\varrho_n>1$, μ is positive, and so the corresponding linear modes are stable. On the contrary, when $\varrho_n<1$, it is possible to make the liquid bridge unstable. What actually happens is decided by the right-hand side of Eq. (22). When $\xi\cos\vartheta_c\leqslant 0$ no linear mode exists; when $\xi\cos\vartheta_c>0$ there are both stable and unstable linear modes, and the latter prevail whenever $|\xi|$, and hence the strength of the line tension $|\gamma|$ is large enough. Thus, the analysis of linear modes can be summarized as follows: If $(R/\xi)\sin\vartheta_c\cos\vartheta_c>1$, then the admissible linear modes have $\varrho_n>1$ and are stable; if $0<(R/\xi)\sin\vartheta_c\cos\vartheta_c<1$,

then the admissible linear modes have $\varrho_n < 1$ and they are unstable.

When $\sigma_n > 0$, the solutions to Eq. (17) that satisfy the symmetry requirement (20) are $u_n(\vartheta) = A \cos\sqrt{\sigma_n}\vartheta$, where the constant A is uniquely determined by Eq. (5): since the boundary condition (19) is homogeneous, A plays no role in the following. We shall refer to these solutions as the *circular* modes. By inserting a circular mode into Eq. (19), after some algebraic manipulations we arrive at the condition

$$\varrho_n = \frac{R}{\xi} \sin\vartheta_c \left(\cos\vartheta_c + \frac{\sin\vartheta_c}{\vartheta_c} x_n \tan x_n \right) =: f_c(x_n), \quad (23)$$

where we have set $x_n := \sqrt{\sigma_n}\vartheta_c$. Similarly, when $\sigma_n < 0$ the solutions to Eq. (17) that also obey Eq. (20) are proportional to $u_n(\vartheta) = \cosh\sqrt{-\sigma_n}\vartheta$. Hereafter, we will refer to these functions as the *hyperbolic* modes. When a hyperbolic mode is inserted into Eq. (19) we readily obtain

$$\varrho_n = \frac{R}{\xi} \sin\vartheta_c \left(\cos\vartheta_c - \frac{\sin\vartheta_c}{\vartheta_c} x_n \tanh x_n \right) =: f_h(x_n), \quad (24)$$

where now we have set $x_n := \sqrt{-\sigma_n}\vartheta_c$. Had we also allowed the odd modes in Eq. (14), only a few specific circular modes would have been selected by the boundary equation (19), all of which could be shown to be stable. Thus, our stability analysis is not restricted by the choice of symmetric perturbations made in Eq. (15).

For a given ϱ_n, both Eqs. (23) and (24) determine the admissible roots x_n, which in turn, through Eq. (21), determine the corresponding eigenvalue μ:

$$\mu R^2 = \varrho_n - 1 \pm \left(\frac{x_n}{\vartheta_c} \right)^2, \quad (25)$$

where the plus and the minus sign apply to circular and hyperbolic modes, respectively. For later reference, we indicate by $\mathcal{Q}$ the positive quadrant in the (x_n, ϱ_n) plane:

$$Q := \{(x_n, \varrho_n), x_n \geqslant 0, \varrho_n \geqslant 0\}.$$

By Eq. (25), the loci in $\mathcal{Q}$ that correspond to a fixed value of μ are parabolas, and parabolas corresponding to different values of μ never intersect each other, as they are obtained from one another by translation along the ϱ_n axis. In particular, the *marginal* parabola obtained from Eq. (25) when $\mu = 0$ for either circular or hyperbolic modes divides $\mathcal{Q}$ into two regions: the region underneath the marginal parabola hosts the pairs (x_n, ϱ_n) for which the associated mode is stable. Parabola (25) is called marginal because it corresponds to marginal stability of the liquid bridge to either circular or hyperbolic modes. The pairs (x_n, ϱ_n) lying on the marginal parabola will play a special role in the graphical discussion of our stability analysis. They represent the points where the graphs of the functions f_c and f_h emanate in both the stable and the unstable manifolds: following the stable branches of these graphs will identify the stable admissible modes ϱ_n.

We now treat separately circular and hyperbolic modes: combining the results of these parallel analyses will lead us to the stability diagram of liquid bridges with both positive and negative line tension. Here we take $\xi > 0$.

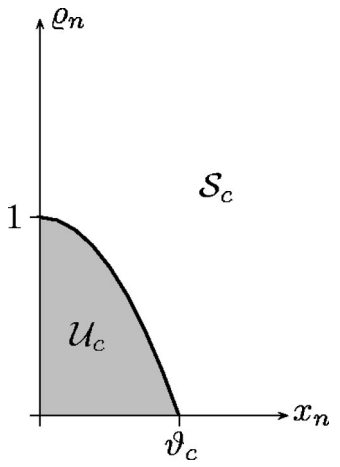

FIG. 2. The marginal parabola (26) divides the positive quadrant $\mathcal{Q}$ into two sets $\mathcal{S}_c$ and $\mathcal{U}_c$. The pairs (x_n, ϱ_n) that belong to $\mathcal{S}_c$ correspond to positive values of μ, whereas the pairs (x_n, ϱ_n) that belong to $\mathcal{U}_c$ correspond to negative values of μ. Given a value of ϱ_n, when the root x_n of Eq. (23) is such that $(x_n, \varrho_n) \in \mathcal{U}_c$, the liquid bridge is unstable against the corresponding circular mode, while it is stable if $(x_n, \varrho_n) \in \mathcal{S}_c$. The parabola (26) is called marginal because it corresponds to marginal stability of the liquid bridge against circular modes.

The equation of the marginal parabola for circular modes is

$$\varrho_n = 1 - \left(\frac{x_n}{\vartheta_c} \right)^2. \quad (26)$$

Whenever a pair (x_n, ϱ_n) that solves Eq. (23) lies in the region $\mathcal{S}_c$ shown in Fig. 2, the corresponding circular mode is stable. On the contrary, when a pair (x_n, ϱ_n) lies in the region $\mathcal{U}_c$, the corresponding circular mode is unstable. The pairs (x_n, ϱ_n) that lie on the marginal parabola (26) are obtained by inserting Eq. (26) into Eq. (23); the following equation then results:

$$1 - \left(\frac{x}{\vartheta_c} \right)^2 = \frac{R}{\xi} \sin\vartheta_c \left(\cos\vartheta_c + \frac{\sin\vartheta_c}{\vartheta_c} x \tan x \right) = f_c(x), \quad (27)$$

where the mode index n has been dropped because the roots of Eq. (27) are independent of n. Since the marginal parabola in $\mathcal{Q}$ is decreasing and f_c has separate increasing branches, the liquid bridge is stable against every circular mode for which

$$\varrho_n > \overline{\varrho} := 1 - \left(\frac{\overline{x}}{\vartheta_c} \right)^2, \quad (28)$$

where $\overline{x}$ is the smallest root of Eq. (27), whenever there is at least one. In such a case, it follows from Eq. (18) that all circular modes are stable provided that the one for $n = 1$ is stable. To seek $\overline{x}$, we consider two different regimes according to whether $\vartheta_c \in (0, \pi/2)$ or $\vartheta_c \in (\pi/2, \pi)$; the limit case $\vartheta_c = \pi/2$ was already discussed in Ref. [9]. When

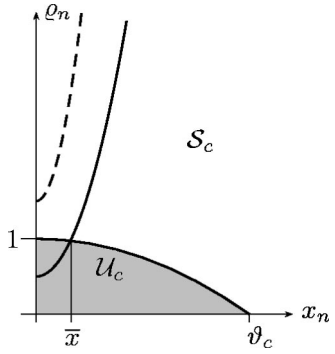

FIG. 3. The graphical solution of Eq. (27) can be obtained by seeking the intersections in $\mathcal{Q}$ between the parabola (26) and the function f_c, when both $\vartheta_c \in (0, \pi/2)$ and $\xi > 0$ are given. Here we have plotted two graphs of the function $f_c(x_n)$: one for $(R/\xi)\sin\vartheta_c \cos\vartheta_c < 1$ (solid curve) and the other for $(R/\xi)\sin\vartheta_c \cos\vartheta_c > 1$ (dashed curve). In the former case, Eq. (27) has a unique root $\overline{x} > 0$ whereas in the latter case it has none.

$\vartheta_c \in (0, \pi/2)$, no intersection between the graph of the function f_c and the parabola (26) exists in the set $\mathcal{Q}$ for

$$\frac{R}{\xi} \sin\vartheta_c \cos\vartheta_c > 1 \tag{29}$$

(see Fig. 3).

Moreover, again by the monotonicity of f_c in $(0, \pi/2)$, we conclude that its graph lies in the stable manifold $\mathcal{S}_c$. Thus, when the inequality (29) holds, the smallest eigenvalue $\mu_{\min}$ is strictly positive, and the bridge is stable against all circular modes. On the contrary, when

$$0 < \frac{R}{\xi} \sin\vartheta_c \cos\vartheta_c < 1 \tag{30}$$

Eq. (27) possesses a unique solution $\overline{x} \in (0, \vartheta_c)$, and (28) is the corresponding stability condition.

Equation (27) has a unique root $x_n \in (0, \pi/2)$ also when $\vartheta_c \in (\pi/2, \pi)$, as shown in Fig. 4, and the stability threshold formally coincides with (28). As an aside, we note that Eq. (27) has no further roots $x \geqslant 0$, when $\vartheta_c \in (\pi/2, \pi)$. In fact, $x \tan x$ is a monotonically increasing function when x is in the range $(\pi/2, \pi)$, so that the function $f_c(x)$ attains its maximum in $(\pi/2, \pi)$ at $x = \pi$, where it has the same, negative value as at $x = 0$.

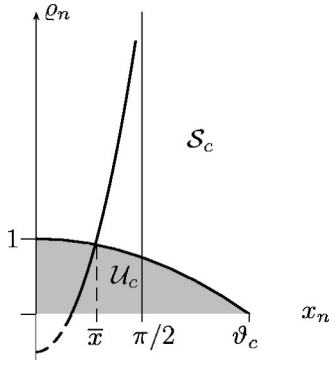

FIG. 4. When $\vartheta_c \in (\pi/2, \pi)$ and $\xi > 0$, Eq. (27) still has a unique root $\overline{x} \in (0, \pi/2)$.

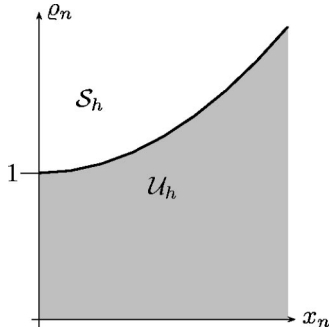

FIG. 5. The parabola (31) divides the positive quadrant $\mathcal{Q}$ into two sets $\mathcal{S}_h$ and $\mathcal{U}_h$. The pairs (x_n, ϱ_n) that belong to $\mathcal{S}_h$ correspond to positive values of μ, whereas the pairs (x_n, ϱ_n) that belong to $\mathcal{U}_h$ correspond to negative values of μ. For given ϱ_n, when the positive solution x_n to Eq. (32) is such that $(x_n, \varrho_n) \in \mathcal{U}_h$, then the liquid bridge is unstable against the corresponding hyperbolic mode, whereas it is stable if $(x_n, \varrho_n) \in \mathcal{S}_h$. The parabola (31) corresponds to marginal stability of the liquid bridge against hyperbolic modes.

To study the hyperbolic modes, we write the marginal parabola in the form

$$\varrho_n = 1 + \left(\frac{x_n}{\vartheta_c}\right)^2. \tag{31}$$

The parabola (31) divides the quadrant $\mathcal{Q}$ into a stable region $\mathcal{S}_h$ and an unstable region $\mathcal{U}_h$, as sketched in Fig. 5.

By inserting Eq. (31) into Eq. (24) we arrive at

$$1 + \left(\frac{x}{\vartheta_c}\right)^2 = \frac{R}{\xi} \sin\vartheta_c \left(\cos\vartheta_c - \frac{\sin\vartheta_c}{\vartheta_c} x \tanh x\right) = f_h(x). \tag{32}$$

Since the marginal parabola is now increasing in $\mathcal{Q}$ while f_h is decreasing, the stability condition (28) is here replaced by

$$\varrho_n > \overline{\varrho} = 1 + \left(\frac{\overline{x}}{\vartheta_c}\right)^2, \tag{33}$$

where $\overline{x}$ is now the unique root of Eq. (32), whenever it exists. We now study Eq. (32) assuming first that $\vartheta_c \in (0, \pi/2)$. When inequality (29) holds, by plotting the graph of the function f_h we readily conclude that Eq. (32) has a unique positive root $\overline{x}$ (see Fig. 6). Although a comparison between the thresholds (28) and (33) would show that hyperbolic modes impose a more stringent requirement on the stability of liquid bridges than circular modes, this is indeed the case only when both Eqs. (27) and (32) possess positive roots, which never happens. When inequality (30) holds, which is the condition for a positive root x_n of Eq. (23) to exist, Eq. (32) has no positive root. Then, the graph of $f_h(x_n)$ lies entirely away from the stable set $\mathcal{S}_h$, and we conclude that the hyperbolic modes for which

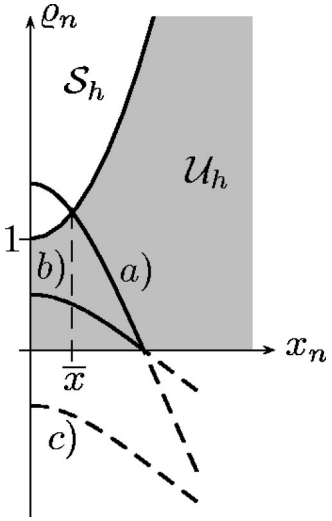

FIG. 6. Graphical solution of Eq. (32). The curve *a* corresponds to the case where $\vartheta_c \in (0, \pi/2)$ and inequality (29) holds: Eq. (32) has a unique positive root $\overline{x}$; liquid bridges satisfying inequality (33) are unstable against hyperbolic modes. The curve *b* corresponds to the case where $\vartheta_c \in (0, \pi/2)$ and inequality (30) holds: Eq. (32) has no positive root, but the graph of the function f_h is entirely outside $\mathcal{S}_h$, and so bridges satisfying inequality (34) are unstable. Finally, the curve *c* corresponds to the case where $\vartheta_c \in (\pi/2, \pi)$: the function $f_h(x)$ is negative when $x \geqslant 0$, and so no hyperbolic mode exists.

$$0 \leqslant \varrho_n < \frac{R}{\xi} \sin \vartheta_c \cos \vartheta_c < 1 \tag{34}$$

make the liquid bridge unstable. Finally, when the contact angle ϑ_c is in $(\pi/2, \pi)$, Eq. (32) has no positive root in $\mathcal{Q}$: since the function $f_h(x)$ is negative for $x \geqslant 0$, no hyperbolic mode exists.

We need now to combine the results of our analysis for all separate modes to arrive at the full stability diagram. This requires examining the role of R/ξ in the preceding conclusions. We first focus attention on the limiting cases where either $R/\xi \ll 1$ or $R/\xi \gg 1$. In particular, we are concerned with the asymptotic behavior of the root $\overline{x}$ to either Eq. (27) or Eq. (32). We defer the details of the asymptotic analysis to the Appendix; here we collect only the results of this analysis.

We first suppose that $\vartheta_c \in (0, \pi/2)$ and that $R/\xi \ll 1$ so that the line tension is dominant and inequality (30) holds. Under these assumptions, the stability limit $\overline{\varrho}$ in Eq. (33) becomes

$$\overline{\varrho} \approx \tan \vartheta_c \left(\frac{R}{\xi} \right). \tag{35}$$

Thus, when the line tension is very large, most circular modes are stable. It is actually sufficient to assume (35) to be valid for $n=1$ to make all circular modes stable. No further analysis is required for the hyperbolic modes, as the instability threshold is still given by inequality (34). We simply note that the thresholds in both inequalities (34) and (35) are linear functions of R/ξ, and that the stability threshold corresponding to circular modes is higher than the stability threshold for hyperbolic modes. Moreover, by Eq. (22), this latter coincides with the locus of instability for linear modes.

In the limiting case where $R/\xi \gg 1$ inequality (29) holds and so circular modes cannot induce instability. As shown in the Appendix, the limit of stability $\overline{\varrho}$ in Eq. (33) approaches the asymptotic value

$$\varrho^\infty := 1 + \left(\frac{\ell}{\vartheta_c} \right)^2, \tag{36}$$

where ℓ is the unique positive root of

$$\ell \tanh \ell = \vartheta_c \cot \vartheta_c. \tag{37}$$

The bound in Eq. (36) represents the supremum of all the values of ϱ_n for which unstable, hyperbolic modes exist. When R/ξ exceeds the critical value

$$\left(\frac{R}{\xi} \right)^* := \frac{1}{\sin \vartheta_c \cos \vartheta_c},$$

which marks the transition between the regimes (29) and (30), the hyperbolic modes smoothly replace the circular modes in driving the bridge's instability. The analysis in the Appendix proves that for R/ξ near $(R/\xi)^*$ the limit of stability $\overline{\varrho}$ reads as

$$\varrho \approx 1 + \frac{1}{1 + \vartheta_c \tan \vartheta_c} \left(\frac{R}{\xi} \sin \vartheta_c \cos \vartheta_c - 1 \right). \tag{38}$$

To obtain the complete stability diagram, we determined numerically the values of the roots $\overline{x}$ to Eqs. (27) and (32), for different values of R/ξ. Collecting together the information contained in Eqs. (22), (28), and (33) and using the analytical estimates (35), (A3), and (38), we obtain the stability diagram of Fig. 7 in which the value $\overline{\varrho}$ of ϱ_n at marginal stability has been plotted against the ratio R/ξ, when $\vartheta_c = 35°$: no relevant changes occur when a different value of ϑ_c is chosen in $(0, \pi/2)$.

Clearly, it follows from Eq. (18) that the inequality $\varrho_n > \overline{\varrho}$ is satisfied for all $n > 1$ provided it is satisfied for $n=1$. Thus, all admissible modes (either circular or hyperbolic) are stable as soon as the first is so. Figure 7 also shows the stabilizing effect of a positive line tension when $\vartheta_c \in (0, \pi/2)$: the larger is ξ, the smaller is $\overline{\varrho}$, and in the limit as $\xi \gg R$ the size L of the destabilizing modes diverges.

When the contact angle $\vartheta \in (\pi/2, \pi)$, only circular modes need to be studied. An analysis that closely parallels the one already performed for $\vartheta_c \in (0, \pi/2)$ (see the Appendix) here leads us to the following asymptotic behaviors for the limit of stability:

$$\varrho \approx 1 - \left(\frac{\pi}{2\vartheta_c} \right)^2 =: \varrho^0 \quad \text{for} \quad \frac{R}{\xi} \ll 1 \tag{39}$$

and

$$\varrho \approx 1 - \left(\frac{\ell}{\vartheta_c} \right)^2 =: \varrho^\infty \quad \text{for} \quad \frac{R}{\xi} \gg 1, \tag{40}$$

where ℓ is the unique positive root in $(0, \pi/2)$ of the transcendental equation

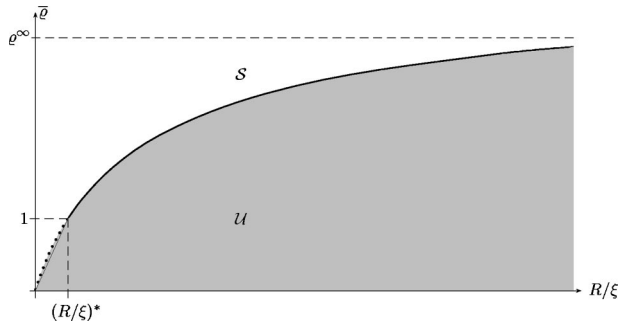

FIG. 7. In this stability diagram we plotted the value $\bar{\varrho}$ of ϱ_n at marginal stability against the dimensionless ratio R/ξ, for $\vartheta_c=35°$. When a pair $(R/\xi,\varrho_n)$ lies in the set $\mathcal{S}$, the liquid bridge is stable against all modes, whereas when a pair $(R/\xi,\varrho_n)$ lies in the set $\mathcal{U}$, the liquid bridge is unstable. When $R/\xi<(R/\xi)^* := 1/\sin\vartheta_c\cos\vartheta_c$, linear, circular, and hyperbolic unstable modes coexist, whereas, when $(R/\xi)>(R/\xi)^*$, only hyperbolic unstable modes survive. According to both (22) and (34), for $(R/\xi)<(R/\xi)^*$ the straight-line segment $\varrho_n=(R/\xi)\sin\vartheta_c\cos\vartheta_c$ marks the onset of instability for both linear and hyperbolic modes (solid thin line). However, the circular modes impose a stricter requirement on the stability of liquid bridges (dotted line). In the limit where $(R/\xi)\gg 1$ the instability region is bounded by the line ϱ^∞, in agreement with the analytic prediction (36).

$$\ell\tan\ell=-\vartheta_c\cot\vartheta_c. \tag{41}$$

Figure 8 illustrates the stability diagram for $\vartheta_c=125°$: similar diagrams can be obtained for all values of $\vartheta_c\in(\pi/2,\pi)$. We note that, at variance with the case where $\vartheta_c\in(0,\pi/2)$, the value $\bar{\varrho}$ of ϱ_n at marginal stability ranges in $(\varrho^0,\varrho^\infty)$ which means that, regardless of the value of R/ξ, it is always possible to make a liquid bridge unstable, provided that ϱ_n is chosen sufficiently small.

In other words, when $\vartheta_c\in(\pi/2,\pi)$, increasing the line tension broadens the stability region, but there always survive unstable modes over a size L sufficiently large.

To compare the limits of stability for liquid bridges to the classical Rayleigh's instability for a full liquid cylinder in the absence of line tension, we recall that this latter would take place at $\bar{\varrho}=1$.

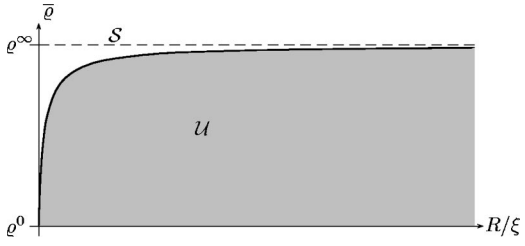

FIG. 8. The value $\bar{\varrho}$ of ϱ_n at marginal stability is plotted against the dimensionless ratio R/ξ, for $\vartheta_c=125°$. When a pair $(R/\xi,\varrho_n)$ lies in the set $\mathcal{S}$, the liquid bridge is stable against all the modes we have examined, whereas when a pair $(R/\xi,\varrho_n)$ lies in the set $\mathcal{U}$, the liquid bridge is unstable against circular modes. Along the curve of marginal stability $\bar{\varrho}$ ranges between $\varrho^0\simeq 0.488$ and $\varrho^\infty\simeq 0.79$ and so, regardless of the value of R/ξ, unstable liquid bridges always exist, provided ϱ_n is chosen sufficiently small.

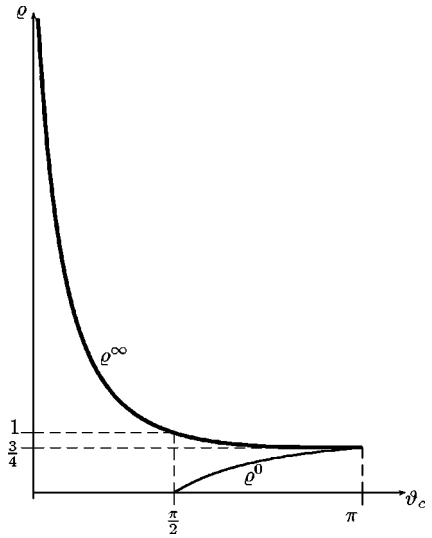

FIG. 9. The graphs of ϱ^∞ against $\vartheta_c\in(0,\pi)$ and of ϱ^0 against $\vartheta_c\in(\pi/2,\pi)$. We note that both ϱ^∞ and ϱ^0 approach the same value 3/4 when $\vartheta_c\to\pi$. While ϱ^∞ diverges when $\vartheta_c\to 0$, $\varrho^0=0$ at $\pi/2$. Moreover, $\varrho^\infty=1$ for $\vartheta_c=\pi/2$, as it should be, on the basis of the classical Rayleigh instability in the absence of line tension.

Figure 9 shows the graph of ϱ^∞ in the whole range $(0,\pi)$ for ϑ_c and that of ϱ^0 for ϑ_c in $(\pi/2,\pi)$. It should be noted that $\varrho^\infty=1$ for $\vartheta_c=\pi/2$, as there Rayleigh's instability must be recovered in the limit $R/\xi\gg 1$.

B. Negative line tension

The scenario we have just outlined applies when the line tension is positive. When the line tension, and hence ξ, is negative substantial changes occur, as we now proceed to show. In fact, Eqs. (27) and (32) can be recast as

$$1-\left(\frac{x}{\vartheta_c}\right)^2=-\frac{R}{|\xi|}\sin\vartheta_c\left(\cos\vartheta_c+\frac{\sin\vartheta_c}{\vartheta_c}x\tan x\right)=-f_c(x) \tag{42}$$

and

$$1+\left(\frac{x}{\vartheta_c}\right)^2=-\frac{R}{|\xi|}\sin\vartheta_c\left(\cos\vartheta_c-\frac{\sin\vartheta_c}{\vartheta_c}x\tanh x\right)=-f_h(x), \tag{43}$$

respectively.

When $\vartheta_c\in(0,\pi/2)$, Eq. (42) has no positive root and the graph of $-f_c$ lies entirely outside $\mathcal{Q}$: we conclude that circular modes are not admissible.

Hyperbolic modes reveal additional interesting features. In fact, when $\vartheta_c\in(0,\pi/2)$, the numerical solution of Eq. (43) shows that no roots exist if $R/|\xi|$ is less than a critical value $(R/|\xi|)_c$ (see Fig. 10), while two roots exist when $R/|\xi|>(R/|\xi|)_c$.

In the former case, the bridge is always unstable since the graph of $-f_h$ lies in the unstable set $\mathcal{U}_h$, whereas in the latter case there exist two values of ϱ_n, namely, $\bar{\varrho}$ and $\varrho^*>\bar{\varrho}$, such that liquid bridges are stable against hyperbolic modes whenever

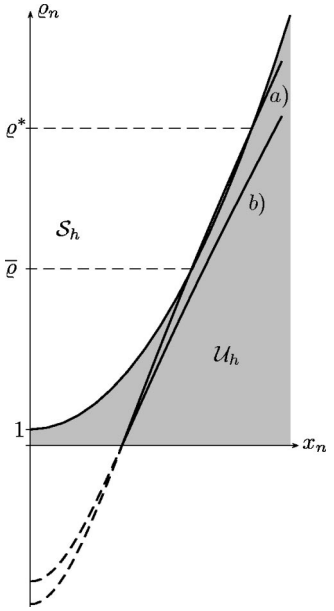

FIG. 10. Graphical solution of Eq. (43) for $\vartheta_c \in (0, \pi/2)$. The curve a has two intersections in $\mathcal{Q}$ with the marginal parabola (31), whereas the curve b has no intersection at all with the same parabola. In the former case, liquid bridges for which $\overline{\varrho} < \varrho_n < \varrho^*$ are stable against hyperbolic modes, whereas in the latter case all liquid bridges are unstable against hyperbolic modes.

$$\overline{\varrho} < \varrho_n < \varrho^* . \tag{44}$$

The left inequality in (44) has the usual interpretation, and it is satisfied for all modes, as long as it is satisfied for $n=1$. More crucially, the right inequality can be satisfied only when the line tension, though negative, is small enough in absolute value. The same asymptotic analysis in the Appendix shows that $\overline{\varrho}$ has formally the same limit as in Eq. (36) with ℓ satisfying Eq. (37), while ϱ^* diverges as

$$\varrho^* \approx \left(\frac{R}{|\xi|}\right)^2 \quad \text{for} \quad \frac{R}{|\xi|} \gg 1. \tag{45}$$

Figure 11 shows the relevant stability diagram for $\vartheta_c = 35°$.

This diagram, which remains qualitatively unchanged for all $\vartheta_c \in (0, \pi/2)$, reveals that liquid bridges are conditionally stable also when the line tension is negative. The intuitive expectation that they would be totally unstable is valid only when the absolute value of the line tension is sufficiently large, that is, for $(R/|\xi|) < (R/|\xi|)_c$. For $(R/|\xi|) > (R/|\xi|)_c$, alongside the upper limit of stability for the length L, which arises from the lower bound in (44) and is related to the classical Rayleigh instability, there is an upper limit on the mode index n arising from the upper bound in (44). This means that, for any given L such that the lower bound in (44) is obeyed for all n, highly wiggly modes eventually make the liquid bridge unstable; however, the corresponding wavelength can be so short as to render these modes physically irrelevant, as is definitely the case for $R/|\xi|$ sufficiently large. Moreover, other stabilizing mechanisms could be at work for

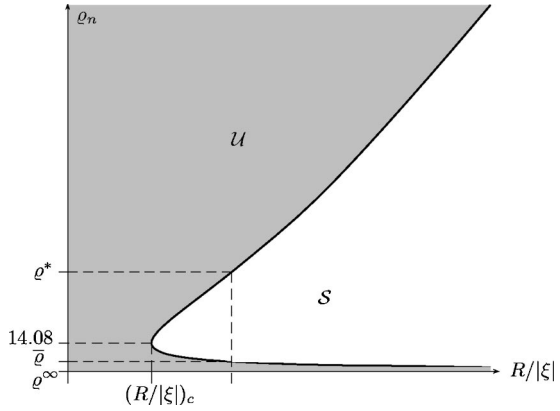

FIG. 11. The values $\overline{\varrho}$ and ϱ^* of ϱ_n at marginal stability are plotted against the dimensionless ratio $R/|\xi|$, for $\vartheta_c = 35°$. When a pair $(R/|\xi|, \varrho_n)$ lies in the set $\mathcal{S}$, the liquid bridge is stable against hyperbolic modes, whereas the liquid bridge is unstable against hyperbolic modes when a pair $(R/|\xi|, \varrho_n)$ lies in the set $\mathcal{U}$. As explained in the text, circular and linear modes are ineffective in this case. For any value of $R/|\xi| > (R/|\xi|)_c \simeq 20.36$, Eq. (43) has two roots. Correspondingly, there are two values of ϱ_n, namely, $\overline{\varrho}$ and ϱ^*, such that liquid bridges are stable whenever $\overline{\varrho} < \varrho_n < \varrho^*$. Clearly, the values of $(R/|\xi|)_c$, $\overline{\varrho}$, and ϱ^* depend on the contact angle ϑ_c. When $\vartheta_c = 35°$ the common value of $\overline{\varrho}$ and ϱ^*, when $(R/|\xi|) = (R/|\xi|)_c$, is $\varrho_n \simeq 14.08$. Finally, the asymptotic value ϱ^∞ formally coincides with that obtained in Eq. (36), with ℓ satisfying Eq. (37).

short wavelengths, especially those related to possible curvature effects on the line tension, which are completely neglected in our mathematical model.

When $\vartheta_c \in (\pi/2, \pi)$, since the function $-f_c(x)$ is decreasing and concave for $x \in (0, \pi/2)$, we conclude that Eq. (42) has a unique root $\overline{x} \in (0, \pi/2)$ if

$$\frac{R}{|\xi|} > \left(\frac{R}{|\xi|}\right)^* := \frac{1}{|\sin \vartheta_c \cos \vartheta_c|}.$$

In this range, stability is guaranteed whenever

$$\varrho_n \geqslant \underline{\varrho} := 1 - \left(\frac{x}{\vartheta_c}\right)^2.$$

If $R/|\xi|$ approaches $(R/|\xi|)^*$ from below, solutions of Eq. (42) exist, provided that $-f_c''(0) = -2(R/|\xi|)\sin^2 \vartheta_c/\vartheta_c$ is larger than the second derivative $-2/\vartheta_c^2$ of the marginal parabola, that is, provided that

$$\frac{R}{|\xi|} < \frac{1}{\vartheta_c \sin^2 \vartheta_c} \tag{46}$$

(see Fig. 12).

In this case, it is possible to find a new critical value $(R/|\xi|)_c$ of $R/|\xi|$ such that Eq. (42) has two roots $\overline{\varrho}$ and ϱ^* for $(R/|\xi|)_c < R/|\xi| < (R/|\xi|)^*$, while it has none for $R/|\xi| < (R/|\xi|)_c$. It turns out that requiring (46) to be satisfied at $R/|\xi| = (R/|\xi|)^*$ is possible only if $-\cot \vartheta_c > \vartheta_c$, inequality which holds for $\vartheta_c \in (\overline{\vartheta}_c, \pi)$, where $\overline{\vartheta}_c \simeq 160°.33 \simeq 2.80$ rad is the root of $-\cot \vartheta_c = \vartheta_c$ in $(0, \pi)$. Accordingly, for

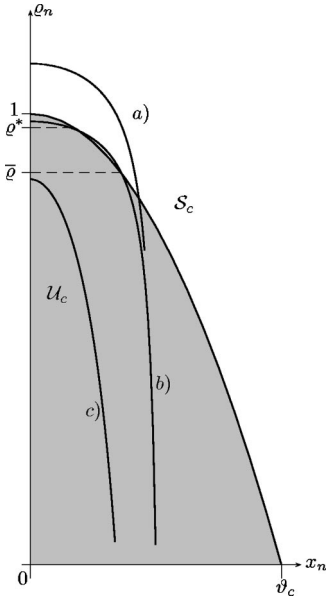

FIG. 12. Graphical solution of Eq. (42) for $\vartheta_c \in (\pi/2, \overline{\vartheta_c})$. The curve *a*, which corresponds to the case where $R/|\xi| > (R/|\xi|)^* = 1/|\sin\vartheta_c \cos\vartheta_c|$, has one intersection at $(\overline{x}, \overline{\varrho})$ in $\mathcal{Q}$ with the marginal parabola (26); correspondingly, liquid bridges with $\varrho_n > \overline{\varrho}$ are stable. Curve *b* corresponds to the case where $(R/|\xi|)_c < R/|\xi| < (R/|\xi|)^*$; here, Eq. (42) has two solutions and only liquid bridges for which $\overline{\varrho} < \varrho_n < \varrho^*$ are stable against circular modes. Finally, when $R/|\xi| < (R/|\xi|)_c$, curve *c*, Eq. (42) has no solution and all liquid bridges are unstable against circular modes. When $\vartheta_c \in (\overline{\vartheta_c}, \pi)$ no curve like *b* exists: all graphs of f_c are like *a* or *c*.

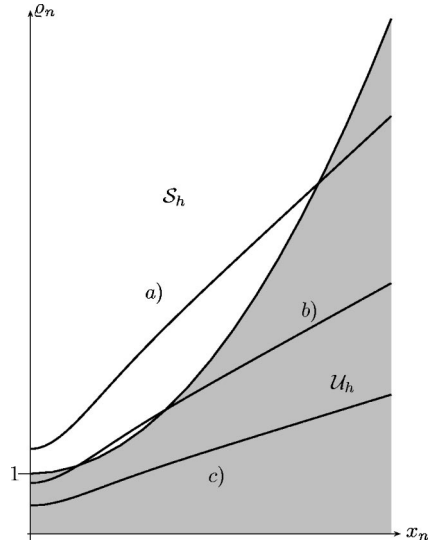

FIG. 13. Graphical solution of Eq. (43), when $\vartheta_c \in (\pi/2, \overline{\vartheta_c})$. The curve *a* corresponds to the regime $(R/|\xi|) > (R/|\xi|)^* := 1/|\sin\vartheta_c \cos\vartheta_c|$, where Eq. (43) has a unique root. The curve *b* corresponds to the regime $(R/|\xi|)_c < R/|\xi| < (R/|\xi|)^*$, where Eq. (43) has two roots, and, finally, the curve *c* corresponds to the regime $(R/|\xi|) < (R/|\xi|)_c$, where Eq. (43) has no root. When $\vartheta_c \in (\overline{\vartheta_c}, \pi)$ no curve like *b* exists: all graphs of f_h are like *a* or *c*.

$(R/|\xi|)_c < R/|\xi| < (R/|\xi|)^*$, only the liquid bridges such that $\overline{\varrho} < \varrho_n < \varrho^*$ are stable against circular modes. Finally, if $R/|\xi| < (R/|\xi|)_c$, Eq. (42) has no root, the graph of $-f_c$ always lies in $\mathcal{U}_c$, and so instability occurs whenever

$$0 < \varrho_n \leqslant \frac{R/|\xi|}{(R/|\xi|)_c} < 1. \tag{47}$$

On the contrary, if inequality (46) is violated at $R/|\xi| = (R/|\xi|)^*$, Eq. (42) has no root for $R/|\xi| < (R/|\xi|)^*$, and so instability occurs whenever

$$0 < \varrho_n \leqslant \frac{R/|\xi|}{(R/|\xi|)^*} < 1. \tag{48}$$

As an aside, we note that no further root to Eq. (42) exists in $(\pi/2, \pi)$, since there f_c is a decreasing function that attains at $x = \pi$ the same positive value as at $x = 0$.

The analysis of Eq. (43) parallels that of Eq. (42), and so we simply collect the relevant results. For $\vartheta_c \in (\pi/2, \overline{\vartheta_c})$, Eq. (43) has no positive root when $R/|\xi| < (R/|\xi|)_c$, it has two positive roots when $(R/|\xi|)_c < R/|\xi| < (R/|\xi|)^*$, and it has a unique root when $(R/|\xi|) > (R/|\xi|)^*$ (see Fig. 13). On the contrary, for $\vartheta_c \in (\overline{\vartheta_c}, \pi)$, Eq. (43) has no positive root when $R/|\xi| < (R/|\xi|)^*$, and it has a unique root when $(R/|\xi|) > (R/|\xi|)^*$.

In the former case, liquid bridges are unstable against hyperbolic modes, regardless of the value of ϱ_n. When Eq. (43) has two roots, there exist two values of ϱ_n, namely, $\overline{\varrho}$ and $\varrho^* > \overline{\varrho}$ such that liquid bridges are stable whenever $\overline{\varrho} < \varrho_n < \varrho^*$. Finally, when there is a single root to Eq. (43), liquid bridges are stable for $1 < R/|\xi|/(R/|\xi|)^* < \varrho_n < \overline{\varrho}$, while hyperbolic modes cease to exist for $\varrho_n < R/|\xi| < (R/|\xi|)^*$.

In the stability diagram shown in Fig. 14 the value of ϱ_n at marginal stability is plotted against $R/|\xi|$, for $\vartheta_c = 125°$. As soon as $(R/|\xi|)$ exceeds $(R/|\xi|)^*$, one branch of hyperbolic modes is smoothly replaced by another branch of circular modes. Although linear modes could here be effective, they lie within the set $\mathcal{U}$, and so they do not constitute an independent source of instability. Had we chosen a value of the contact angle in $(\overline{\vartheta_c}, \pi)$, the stability diagram would be equivalent to that shown in Fig. 14; the only difference would be that a branch of circular modes is smoothly replaced by another branch of hyperbolic modes as soon as $(R/|\xi|)$ exceeds $(R/|\xi|)^*$. Needless to say, $\overline{\varrho}$ and ϱ^* depend on both $R/|\xi|$ and the contact angle ϑ_c. The asymptotic value of $\overline{\varrho}$ is still given by Eq. (40) with ℓ as in Eq. (41), while ϱ^* diverges as

$$\varrho^* \approx \left(\frac{R}{|\xi|}\right)^2 \quad \text{for} \quad \frac{R}{|\xi|} \gg 1.$$

Also when $\vartheta_c \in (\pi/2, \pi)$ there is a critical value $(R/|\xi|)_c$ for $R/|\xi|$ below which all existing modes are unstable; this means that a large, negative line tension causes instability of all liquid bridges.

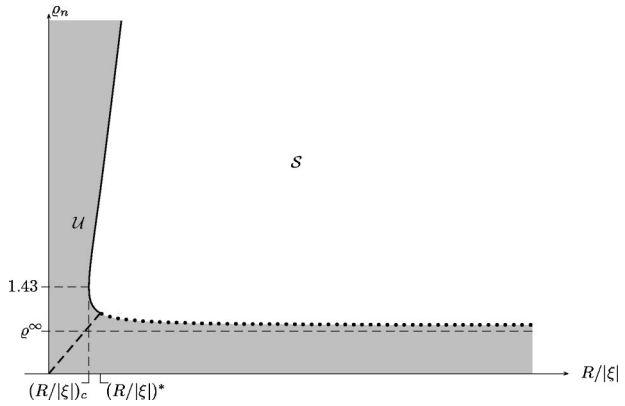

FIG. 14. The value of ϱ_n at marginal stability is plotted against the dimensionless ratio $R/|\xi|$, for $\vartheta_c=125°$. The dashed line marks the onset of instability caused by both linear and circular modes, the dotted line corresponds to circular modes when $R/|\xi|>(R/|\xi|)^* := 1/|\sin\vartheta_c \cos\vartheta_c|$, and, finally, the solid line corresponds to hyperbolic modes. When $1.66\simeq(R/|\xi|)_c<R/|\xi|<(R/|\xi|)^*$ two distinct branches of hyperbolic modes exist while, as soon as $(R/|\xi|)>(R/|\xi|)^*$, one branch is replaced by the circular modes. When a pair $(R/|\xi|,\varrho_n)$ lies in the set $\mathcal{S}$, the liquid bridge is stable, whereas it is unstable when a pair $(R/|\xi|,\varrho_n)$ lies in the set $\mathcal{U}$. The line $\varrho_n=R/|\xi|(R/|\xi|)^*$ divides the stable region $\mathcal{S}$ into two subregions: above this line both hyperbolic and circular modes exist; below this line, only circular modes survive. For $\vartheta_c=125°$ the value of ϱ_n at marginal stability when $R/|\xi|=(R/|\xi|)_c$ is $\varrho_n\simeq1.43$; in general it depends on the contact angle ϑ_c. On the contrary, the value of ϱ_n at marginal stability when $R/|\xi|=(R/|\xi|)^*$ is always $\varrho_n=1$, regardless of the value of ϑ_c. The asymptotic value ϱ^∞ formally coincides with that obtained in Eq. (40), with ℓ now satisfying Eq. (41).

Figure 15 shows the graph of $(R/|\xi|)_c$ as a function of ϑ_c in the whole range $(0,\pi)$. As a rule, the lower $(R/|\xi|)_c$, the larger is the region of stability. The divergence of $(R/|\xi|)_c$ at both $\vartheta_c=0$ and $\vartheta_c=\pi$ follows from our assumption that the line tension and the contact are mutually independent. In fact, they both depend on the temperature and, on approaching either the wetting transition, at $\vartheta_c=0$, or the dewetting transition, at $\vartheta=\pi$, our assumption is questionable. The stability of liquid bridges near wetting and dewetting transitions will form the subject of a forthcoming paper [15].

IV. CONCLUSIONS

We applied the general criterion established in Ref. [9] (see also Ref. [10] for more mathematical details) to the stability of straight liquid bridges on a flat substrate in the presence of line tension. Guided by the classical Rayleigh instability, which should be exactly reproduced in this context when the line tension τ vanishes and the contact angle ϑ_c equals $\pi/2$, one would expect that a liquid bridge becomes unstable when it is sufficiently slender. Intuitively, a positive line tension is expected to have a stabilizing effect, whereas a negative line tension is expected to have a destabilizing effect. Here we proved some of these intuitive predictions to be false.

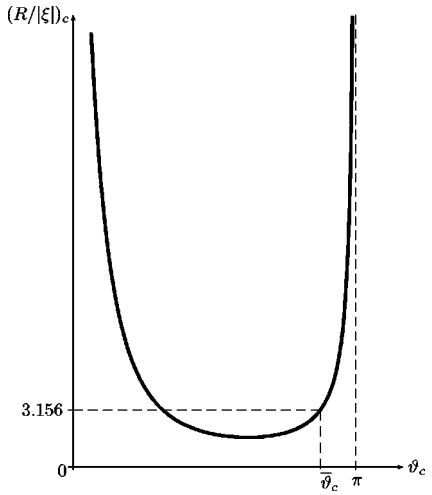

FIG. 15. The value of $(R/|\xi|)_c$ against $\vartheta_c\in(0,\pi)$ diverges as $\vartheta_c\to0$ and as $\vartheta_c\to\pi$. For $0<\vartheta_c<\bar{\vartheta}_c$, $(R/|\xi|)_c$ is computed on hyperbolic modes, whereas it is computed on circular modes for $\bar{\vartheta}_c<\vartheta_c<\pi$. At $\vartheta_c=\bar{\vartheta}_c$, $(R/|\xi|)_c=(R/|\xi|)^*=1/|\sin\bar{\vartheta}_c\cos\bar{\vartheta}_c|$. Here $\bar{\vartheta}_c\cong160°.33\cong2.80$ rad is the root in $(0,\pi)$ of the equation $-\cot\vartheta_c=\vartheta_c$.

In our conclusions a prominent role is played by the contact angle ϑ_c. When $\vartheta_c\in(0,\pi/2)$, a positive line tension has the expected stabilizing effect, as the stability region in the phase diagram broadens when the line tension increases. When $\vartheta_c\in(\pi/2,\pi)$, however, even for a positive, increasing line tension the limit of stability does not grow accordingly: a liquid bridge definitely remains unstable when it is sufficiently slender.

The most surprising results were found here when the line tension is negative. In such a case, if the line tension is not too large in absolute value, there exist a whole variety of stable equilibrium configurations: liquid bridges are still unstable if too slender or subject to perturbations with sufficiently short wavelengths, but both these limitations can fail to be very stringent. This qualitative conclusion easily becomes quantitative through the combination of graphical and numerical methods illustrated in Sec. III A. The same conclusion, however, is not valid for all values of a negative line tension: when the absolute value of the line tension exceeds a critical value, all possible liquid bridges become unstable. Our study has shown that the generic claim that a negative line tension would make all droplets unstable [6–8] is in general false, as already feared [14], since there are at least plenty of conditionally stable liquid bridges.

Other important issues of wetting science have not been addressed here. As remarked in Sec. III B, we have treated the contact angle ϑ_c and the line tension γ as independent from one another. This hypothesis is acceptable only far from the wetting or dewetting transition, where $\vartheta_c\simeq0$ and $\vartheta_c\simeq\pi$, respectively. In fact, when either phase transition is approached, the dependence of both ϑ_c and γ on the temperature becomes relevant, and it is no longer justified to treat ϑ_c and γ as mutually independent. The stability analysis of liquid bridges near both wetting and dewetting transitions will be the object of a future study [15].

Finally, we are aware that our conclusions depend clearly on the special geometry of droplets we considered. We expect that qualitatively different results could follow from applying our stability criterion to droplets of different shape or sitting on substrates that fail to be flat.

APPENDIX: ASYMPTOTIC ANALYSES

We collect here the details of the asymptotic analyses involved in Sec. III A. For convenience, we take ϑ_c first in $(0,\pi/2)$ and then in $(\pi/2,\pi)$

Case $\vartheta_c \in (0,\pi/2)$

To study the asymptotic behavior of the positive root $\bar{x}$ to Eqs. (27) and (32) we adopt the method of dominant balance (see, e.g., Ref. [16], Chap. 3). As a putative behavior for the root $\bar{x}$ when $R/\xi \ll 1$, we assume the following:

$$\bar{x} \sim a\left(\frac{R}{\xi}\right)^{\alpha}, \tag{A1}$$

and then we examine the consequences of this assumption by inspecting the leading terms in either Eq. (27) or Eq. (32). It turns out that there is a unique value of α which leads to a consistent balance, yielding an accurate estimate of the asymptotic behavior of $\bar{x}$.

By inserting the ansatz (A1) into Eq. (27), where both a and α are positive, we suddenly arrive at the inconsistent dominant balance

$$1 = \frac{R}{\xi}\sin\vartheta_c\cos\vartheta_c \ll 1.$$

Since $\bar{x}$ cannot exceed $\pi/2$, a further possibility is assuming $\alpha=0$, that is, $\bar{x}\simeq\ell<\pi/2$. With this assumption Eq. (27) turns into

$$1-\left(\frac{\ell}{\vartheta_c}\right)^2 = \frac{R}{\xi}\sin\vartheta_c\left(\cos\vartheta_c + \frac{\sin\vartheta_c}{\vartheta_c}\ell\tan\ell\right),$$

which is consistent only if $\ell=\vartheta_c$, so that the left-hand side vanishes. To gain further insight into the problem, we suppose that

$$\bar{x} \sim \vartheta_c\left[1-b\left(\frac{R}{\xi}\right)^{\beta}\right] \tag{A2}$$

and we seek for the admissible pairs (b,β), with both b and β positive. By inserting Eq. (A2) into Eq. (27), it readily follows that $\beta=1$ and $b=(1/2)\tan\vartheta_c$. Thus, we arrive at inequality Eq. (35).

Let now $R/\xi \gg 1$. To study Eq. (32) we assume that either $\bar{x}\sim a(R/\xi)^{\alpha}$, $\bar{x}\sim a(R/\xi)^{-\alpha}$, or $\bar{x}\sim\ell>0$, where a and α are positive numbers to be determined. The first assumption leads to the balance

$$\frac{1}{\vartheta_c^2}\left(\frac{R}{\xi}\right)^{2\alpha} = -\frac{\sin^2\vartheta_c}{\vartheta_c}\left(\frac{R}{\xi}\right)^{(\alpha+1)},$$

which is clearly inconsistent because of the sign opposition. The second assumption leads to the inconsistent balance $1=(R/\xi)\sin\vartheta_c\cos\vartheta_c$, whereas the limiting behavior $\bar{x}\sim\ell$ is consistent, provided that ℓ is the unique root of the transcendental equation (37). To gain more insight into this asymptotics, we set $\bar{x}=\ell-a(R/\xi)^{-\delta}$, for positive a and δ, and we match further terms in Eq. (32). By use of Eq. (37), we obtain

$$1+\left(\frac{\ell}{\vartheta_c}\right)^2 - \frac{2}{\vartheta_c^2}a\ell\left(\frac{R}{\xi}\right)^{-\delta} = a\frac{\sin^2\vartheta_c}{\vartheta_c}\left(\tanh\ell+\ell(1-\tanh^2\ell)\right)\times\left(\frac{R}{\xi}\right)^{(1-\delta)},$$

where the right-hand side of Eq. (32) has been expanded near $\bar{x}=\ell$. Hence, the matching procedure yields $\delta=1$ and

$$a = \frac{1+(\ell/\vartheta_c)^2}{(\sin^2\vartheta_c/\vartheta_c)[\tanh\ell+\ell(1-\tanh^2\ell)]},$$

whence, by Eq. (33), we express the limit of stability $\bar{\varrho}$ as

$$\bar{\varrho} = 1+\left(\frac{\ell}{\vartheta_c}\right)^2 - \frac{2\ell}{\vartheta_c}a\left(\frac{R}{\xi}\right)^{-1} + O\left(\frac{R}{\xi}\right)^{-2}. \tag{A3}$$

Finally, we explore analytically the limiting case where $(R/\xi)\sin\vartheta_c\cos\vartheta_c\to 1$ from either sides, to study the transition between the regimes Eqs. (29) and (30). When $(R/\xi)\sin\vartheta_c\cos\vartheta_c=1-\varepsilon$, a glance at Fig. 3 suffices to justify the ansatz $\bar{x}\sim a\varepsilon^{\gamma}$ in Eq. (27), for positive and yet unknown coefficients a and γ. A consistent balance holds provided that $\gamma=\frac{1}{2}$ and

$$a = \frac{\vartheta_c}{\sqrt{1+\vartheta_c\tan\vartheta_c}}.$$

Correspondingly, $\bar{\varrho}$ in Eq. (33) is given by

$$\bar{\varrho} \approx 1 - \frac{\varepsilon}{1+\vartheta_c\tan\vartheta_c},$$

which is the same as Eq. (38). Formally, the same result is also obtained for hyperbolic modes in the limit where $(R/\xi)\sin\vartheta_c\cos\vartheta_c=1+\varepsilon$.

Case $\vartheta_c \in (\pi/2,\pi)$

When $R/\xi \ll 1$, it is not difficult to prove that we must assume $\bar{x}\to\pi/2$ in such a way that $\tan\bar{x}\sim a(R/\xi)^{-\beta}$, with $a,\beta>0$. Inserting this ansatz into Eq. (27), we readily obtain that $\beta=1$, and

$$a = \frac{1 - \left(\frac{\pi}{2\vartheta_c}\right)^2}{\sin^2 \vartheta_c \left(\frac{\pi}{2\vartheta_c}\right)}.$$

Correspondingly, $\overline{\varrho}$ in inequality (33) reads as in Eq. (39).

A similar analysis in the limiting case where $R/\xi \gg 1$ shows that $\overline{x}$ behaves like $\overline{x} \sim \ell + a(R/\xi)^{-1}$, where

$$a = \frac{\vartheta_c[1 - (\ell/\vartheta_c)^2]}{\sin^2 \vartheta_c[\tan \ell + \ell(1 + \tan^2 \ell)]}$$

and ℓ is the unique root in $(0, \pi/2)$ of the transcendental equation (41). This gives $\overline{\varrho}$ in (33) the asymptotic behavior in Eq. (40).

[1] J.W. Gibbs, *The Collected Papers of J. Willard Gibbs* (Yale University Press, London, 1957).
[2] J.Y. Wang, S. Betelu, and M.B. Law, Phys. Rev. Lett. **83**, 3677 (1999).
[3] T. Pompe and S. Herminghaus, Phys. Rev. Lett. **85**, 1930 (2000).
[4] T. Pompe, Phys. Rev. Lett. **89**, 076102 (2002).
[5] A. Checco, P. Guenoun, and J. Daillant, Phys. Rev. Lett. **91**, 186101 (2003).
[6] D. Li and D.J. Steigmann, Colloids Surf., A **116**, 25 (1996).
[7] D.J. Steigmann and D. Li, IMA J. Appl. Math. **55**, 1 (1995).
[8] D. Li, Colloids Surf., A **116**, 1 (1996).
[9] R. Rosso and E.G. Virga, Phys. Rev. E **68**, 012601 (2003).
[10] R. Rosso and E.G. Virga, J. Phys. A **37**, 3989 (2004).
[11] R. Lipowsky, Interface Sci. **9**, 105 (2001).
[12] I.M. Gelfand and S.V. Fomin, *Calculus of Variations* (Prentice-Hall, Englewood Cliffs, NJ, 1963).
[13] R.V. Roy and R.W. Schwartz, J. Fluid Mech. **391**, 293 (1999).
[14] R. Lipowsky, P. Lenz, and P.S. Swain, Colloids Surf., A **161**, 3 (2000).
[15] R. Rosso (unpublished).
[16] C.M. Bender and S.A. Orszag, *Advanced Mathematical Methods for Scientists and Engineers: Asymptotic Methods and Perturbation Theory* (Springer, Heidelberg, 1999).